УДК 532.528

SUPERCAVITATING VEHICLE MANEUVERING WITH DELAY AND NON-STEADY PLANING

V. NGUYEN, B. BALACHANDRAN

Department of Mechanical Engineering, University of Maryland,
College Park, MD 20742 USA
vince1@umd.edu

In this article, a general form of pitch-plane model for supercavitating vehicle dynamics is presented and used to study vehicle maneuvers. Vehicle motions into and out of the cavity are also considered and this allows for modeling of damping-force like components encountered during planing. The non-steady nature of the planing formulation allows for appropriate treatment of transient vehicle to cavity interactions. Since the vehicle planes on a cavity that is generated by previous cavitator positions, the memory effects play an important role in the model development. Unlike previous models, which are primarily intended for studies of vehicle motions in steady horizontal travel, the current form of the model makes it possible to evaluate transient maneuvers that may deviate considerably from straight and level trajectories. A numerical optimal-control approach is utilized to generate control inputs for maneuvers intended to reach a particular location. Comparisons with previous approaches are made and results obtained for maneuvering are included in this work.

KEY WORDS: supercavitating vehicle, dynamics, maneuvering, delay system, optimal control

В статті описано узагальнену математичну модель динаміки суперкавітуючого апарату у вертикальній площині, яка використовується для дослідження маневреності апарата. Для розрахунку компонент демпфіруючої сили при глісуванні розглянуто рух апарата усередині і зовні каверни. При розгляданні взаємодії апарата з каверною враховується нестаціонарна природа глісування і ефект пам'яті каверни. На відміну від попередніх математичних моделей, які призначались в основному для вивчення стаціонарного горизонтального руху апаратів, запропонована модель дозволяє розглядати маневри апарата з суттєвим відхиленням від прямолінійних траєкторій. Для генерації керуючих сигналів для маневрів, що призначені для досягнення заданого положення, застосовано чисельні методи оптимального управління. Також у роботі дано порівняння з попередніми підходами і наведено результати розрахунків маневрування суперкавітуючого апарата.

КЛЮЧОВІ СЛОВА: суперкавітуючий апарат, динаміка, маневрування, система з запізнюванням, оптимальне управління

В статье описана обобщенная математическая модель динамиики суперкавитирующего аппарата в вертикальной плоскости, которая используется для исследования маневренности аппарата. Для расчета компонент демпфирующей силы при глиссировании рассмотрено движение аппарата внутри и вне каверны. При рассмотрении взаимодействия аппарата с каверной учитывается нестационарная природа глиссирования и эффект памяти каверны. В отличие от предыдущих математических моделей, которые предназначались в основном для изучения стационарного горизонтального движения аппаратов, предлагаемая модель позволяет рассматривать маневры аппарата с существенным отклонением от прямолинейных траекторий. Для генерации управляющих сигналов для маневров, предназначенных для достижения заданного положения, применены численные методы оптимального управления. Также в работе дано сравнение с предыдущими подходами и приведены результаты расчетов маневрирования суперкавитирующего аппарата.

КЛЮЧЕВЫЕ СЛОВА: суперкавитирующий аппарат, динамика, маневрирование, система с запаздыванием, оптимальное управление

Nomenclature

L	Length of vehicle (m)
σ	Cavitation number
α	Immersion angle (rad)
δ_e	Fin deflection angle (rad)
δ_c	Cavitator deflection angle (rad)
C_D	Coefficient of drag
R_C	Cavity radius (m)
V	Vehicle total speed (m/s)
z	Depth (m)
w	Transverse speed (m/s)
θ	Pitch angle (rad)
q	Pitch rate (rad/s)
x_τ	Delayed version of $x(t)$: $x(t - \tau)$
R_n	Cavitator radius (m)
R	Body radius (m)
m	Vehicle mass (kg)
n	Fin effectiveness
C_{x_0}	Cavitator lift coefficient
g	Acceleration due to gravity (m/s^2)

INTRODUCTION

Supercavitation, which can occur during the motions of high-speed underwater vehicles, is defined as a state wherein a gaseous bubble completely
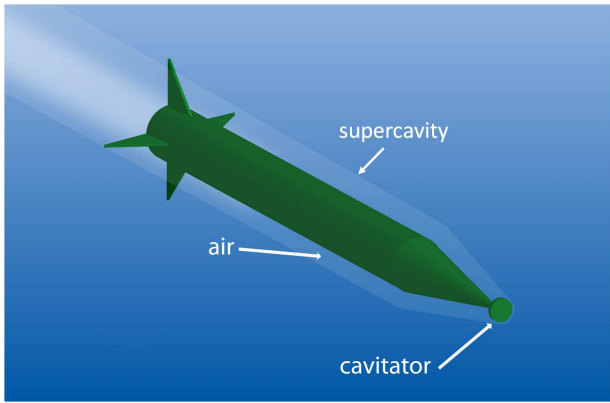
Fig. 1. Illustration of a supercavitating vehicle

envelops the vehicle body, as illustrated in Fig. 1. The advantage of such form of locomotion is increased speed due to reduced skin friction drag. The gas bubble can be either formed through vaporous cavitation generated by the high-speed propulsion alone or aided by forced ventilation. Spurred by the fundamental efforts of Logvinovich [1, 2], considerable progress has been made in modeling complex cavity dynamics. However, the development of accurate models that describe the cavity shape, growth, and collapse is still an open area of research. Vehicle-cavity interactions also pose significant challenges to modeling and analysis of system dynamics and control. These interactions are characterized by strong non-linear planing forces. Since the unwetted vehicle regions do not generates buoyancy forces, these strong interaction forces can arise even during straight and level flight. Due to the intermittent contact with the cavity surface, vehicle stability needs to be carefully addressed. Cavity memory effects also add additional complexity to the system. The cavity surface is generated as the cavitator at the front of the vehicle moves through the fluid. Cavity contact or planing generally occurs at the rear of the vehicle, and the cavity planing surface at this location is generated by previous cavitator positions. Therefore, there is an associated time lapse between when the cavity is created and when it affects the planing forces. This time delay relates approximately to the amount of time it takes the vehicle to move one body length.

Several models have been proposed to study the dynamics of supercavitating vehicles. A supercavitating vehicle of the type considered here is shown in Fig. 1. The hydrodynamic forces applied to the body arise from the control surfaces (the cavitator and fins) and the planing forces that arise when the aft of the body enters the water. Four-state rigid-body models have been used to study pitch-plane dynamics and stability in earlier studies [3 – 8]. A twelve-state rigid-body model is presented in the work [9], and models that reflect the effect of time delay have been examined in the studies [10 – 12]. A numerical model incorporating structural elasticity is presented in the reference [13]. Trajectory optimization for supercavitating vehicles is presented in recent studies [14,15]. In these efforts, time-delay effects are included, but the resulting maneuvers do not utilize planing unlike the current effort.

As mentioned earlier, there have been several studies that have been pursued with the aim of understanding the dynamics of supercavitating vehicles [2, 3, 9]. Of particular relevance to this work, stabilization, control, and maneuvering of supercavitating vehicles have been studied from several points of view in recent years [3, 6 – 9, 11]. Primary differences amongst these models can be summarized in terms of the following features: i) cavity geometry and dynamics and ii) the calculation of planing forces. It is important to note that the results of such studies hinge on the dynamic models used and assumptions inherent in these models. An important aspect of the modeling efforts is the computation of the planing force. In almost all of the studies to date, an approach similar to the one presented in [3] is utilized, in which the planing force is assumed to be the result of fluid transport into a spray sheet, and it is calculated based on an extension of the Wagner planing theory [2].

To the best of the authors' knowledge, in all of the current existing research, cavity interaction forces are calculated by utilizing an assumption of steady-planing. With this approach, the cavity interaction force experienced by the vehicle is estimated as the force experienced by a vehicle body in steady planing along the cavity. The steady planing force allows for computational ease, since the planing force is only based on the geometric positions of the vehicle and the cavity. The steady planing assumption is useful when investigating stability or cases wherein the motions do not deviate greatly from steady state.

Here, the authors present a model for vehicle dynamics on the pitch-plane, and in this model developing, the planing force modeling allows for vehicle motions into or out of the cavity. Since this model accounts for both the geometric positions as well as vehicle speeds into the cavity, this approach can be considered for incorporating the damping-type effects associated with the planing force. These damping-type effects are inherently missing from steady planing formulations. Also, included in the current model is a detailed treatment of the time-

delay effect. The detailed cavity tracking along with the new planing force model allows for consideration of motions that may deviate greatly from steady-state flight. Investigations into maneuvering are presented by utilizing a numerical optimization approach for generating control inputs for the defined maneuvers. Homing maneuvers are presented, and contrary to previous optimal control studies, the resulting vehicle trajectories utilize planing for aggressive vehicle maneuvers.

The rest of the paper is organized as follows. In Section 1, the basic pitch-plane dynamics model is presented. In this section, the vehicle dynamics model, cavity model, and planing force model are developed and discussed. The inclusion of cavity delay effects are discussed in Section 2 along with simulation results obtained with the new model. Details on the maneuvering scheme and associated results obtained are covered in Section 3.

1. DIVE PLANE MODELING

The vehicle dynamics model used in this work is based on a formulation presented in previous studies [3, 5]. The vehicle motions of interest are in the vertical plane or the pitch plane, which is defined by using by the vehicle velocity vector and the vertical axis. A set of equations of motion that can be used to describe the vehicle dynamics are given by Eqs. (1) and (2).

$$\begin{pmatrix} \dot{z} \\ \dot{w} \\ \dot{\theta} \\ \dot{q} \end{pmatrix} = \begin{pmatrix} 0 & 1 & -V & 0 \\ 0 & a_{22} & 0 & a_{24} \\ 0 & 0 & 0 & 1 \\ 0 & a_{42} & 0 & a_{44} \end{pmatrix} \begin{pmatrix} z \\ w \\ \theta \\ q \end{pmatrix} +$$

$$\begin{pmatrix} 0 & 0 \\ b_{21} & b_{22} \\ 0 & 0 \\ b_{41} & b_{42} \end{pmatrix} \begin{pmatrix} \delta_e \\ \delta_c \end{pmatrix} + \begin{pmatrix} 0 \\ c_2 \\ 0 \\ 0 \end{pmatrix} + \quad (1)$$

$$\begin{pmatrix} 0 \\ d_2 \\ 0 \\ d_4 \end{pmatrix} F_p ,$$

$$a_{22} = \frac{CVT}{m}\left(\frac{-1-n}{L}\right)S + \frac{17}{36}nL,$$

$$a_{24} = VTS\left(C\frac{-n}{m} + \frac{7}{9}\right) - VT\left(C\frac{-n}{m} + \frac{17}{36}\right)\frac{17}{36}L^2,$$

$$a_{42} = \frac{CVT}{m}\left(\frac{17}{36} - \frac{11n}{36}\right),$$

$$a_{44} = \frac{-11CVTnL}{36m},$$
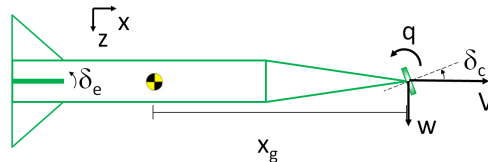

Fig. 2. Coordinate system definition for system model

$$b_{21} = \frac{CV^2Tn}{m}\left(\frac{-S}{L} + \frac{17L}{36}\right), \quad b_{22} = \frac{-CV^2TS}{mL},$$

$$b_{41} = \frac{-11CV^2Tn}{36m}, \quad b_{42} = \frac{17CV^2T}{36m},$$

$$c_2 = g, \quad d_2 = \frac{T}{m}\left(\frac{-17L}{36} + \frac{S}{L}\right),$$

$$d_4 = \frac{11T}{36m}x_p/L, \quad S = \frac{11}{60}R^2 + \frac{133L^2}{405},$$

$$T = \frac{1}{7S/9 - 289L^2/1296},$$

$$C_x = C_{x0}(1 + \sigma), \quad C = 0.5C_x\frac{R_n^2}{R^2}. \quad (2)$$

In this representation, the system dynamics is tracked by using four states, the vertical position z, the transverse velocity w, the pitch angle θ, and the pitch rate q. All of these states are considered at the vehicle nose. The vehicle forward speed, V, is assumed to be constant, and the transverse velocity, w, is taken about a moving coordinate system that follows the vehicle and this velocity component direction is always normal to the vehicle axis (see Fig. 2). The vertical position z is taken about an inertial reference frame, and the pitch angle θ is taken about horizontal. The control inputs are the cavitator and fin (elevator) actuation angles, δ_c and δ_e, respectively. The forces generated by these control surfaces are assumed to be linearly related to their respective angles of attack, with the variable n representing the ratio of the effectiveness of the fins to the cavitator. With additional small angle assumptions, the equations of motion are linear with the exception of the planing force, F_p, which has a non-smooth description. A schematic of a supercavitating vehicle showing the various forces acting on the vehicle body is shown in Fig. 3. The planing force, the fin force, and the cavitator force are applied with respect to the body reference frame. Further details on the assumptions used in deriving the various vehicle forces can be found in earlier studies (e.g., [3, 5]). This set of equations are used as a basis in this work.

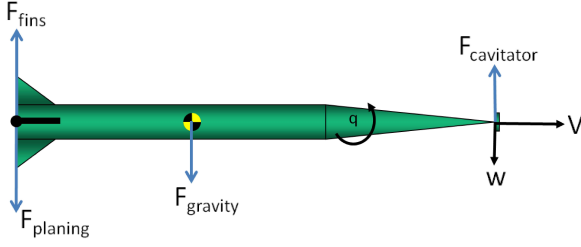### 1.1. Logvinovich and cavity modeling

V. Nguyen, B. Balachandran

Fig. 3. Forces acting on a supercavitating vehicle

The cavity shape is calculated by using the non-dimensional cavitation number σ, which characterizes the extent of cavitation. The cavitation number is given by Eq. 3, where p_∞ is the ambient pressure, p_c is the cavity pressure, ρ is the fluid density, and V is the vehicle speed:

$$\sigma = \frac{p_\infty - p_c}{0.5\rho V^2}. \tag{3}$$

The cavity model is a semi-empirical closed-form solution, which has been derived from a formulation presented in Logvinovich's work [1]. He presented a formulation for the radius of a stationary cavity section for a disc shaped cavitator as it expands and contracts through time. This can be translated to the spatial cavity profile with respect to the cavitator for an axi-symmetric flow. The cavity profile is generated by evaluating the cavity radius along several points by using Eq. (4), where x represents the length from the cavitator, and d_c represents the cavitator diameter, as shown in Fig. 4. Similarly the cavity contraction/growth rate $\dot{R}_c$ can be determined as shown in Eq. (5).

$$
\begin{aligned}
d_{max} &= d_c\sqrt{0.82(1+\sigma)/\sigma}, \\
l_m &= d_c/2(1.92/\sigma - 3), \\
k_1 &= 1.92(0.82(1+\sigma)/\sigma)^{-\frac{1}{2}}, \\
k_2 &= (x \cdot d_c - d_c)/l_m, \\
R_c(x) &= d_{max}/2\sqrt{1 - (1-k_1^2)|1-k_2|^{2/0.85}}, (4)
\end{aligned}
$$

$$\dot{R}_c(x) = \frac{(d_{max}/2)^2}{R_c(x)l_m/V}(1-k_1)\times \tag{5}$$

$$\times\frac{1}{0.85}(1-k_2)|1-k2|^{\frac{2(1-0.85)}{0.85}}.$$

1.2. Planing force modeling

The planing force model is based on a formulation developed by Paryshev [16]. In this work, forces are
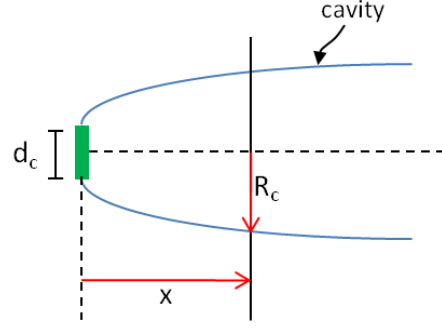

Fig. 4. Cavity model

defined for an expanding cylinder planing on a cylindrical cavity. The force per unit length is determined by evaluating the rate of change of momentum of the fluid displaced by the planing cylinder. This is shown in Eq. (6), where m_y^* represents the apparent mass due to the planing, and m_R^* is the apparent mass due to the expansion of the cylinder. For application to supercavitating vehicles, since the radius of the body does not change, the contribution of the m_R^* can be ignored. The expression for the force can then be expanded as shown in Eq. (7). If there is no acceleration into or out of the fluid, the second term involving $\frac{dV_y}{dt}$ can be dropped.

$$f = \frac{d}{dt}\left(m_y^*V_y + m_R^*\tilde{V}_R\right), \tag{6}$$

$$f = \frac{dm_y^*}{dt}V_y + m_y^*\frac{dV_y}{dt}, \tag{7}$$

$$m_y^* = \pi\rho r^2 h\left(\frac{2\Delta + h}{(\Delta + h)^2}\right), \tag{8}$$

$$\frac{dm_y^*}{dt} = \frac{\partial m_y^*}{\partial h}\frac{dh}{dt} + \frac{\partial m_y^*}{\partial \Delta}\frac{d\Delta}{dt}, \tag{9}$$

$$\frac{dm_y^*}{dh} = 2\pi r^2\rho\Delta^2(\Delta + h)^{-3}, \tag{10}$$

$$F_P = \int\frac{dm_y^*}{dh}\dot{h}^2ds. \tag{11}$$

The expression for the apparent mass, m_y^*, is given in Eq. (8), and this quantity is a function of the immersion depth, h, and the gap, Δ, which is defined as the difference between the cavity radius and the body radius. The rate of change of the apparent mass m_y^* can then be described as shown in Eq. (9). Since the radius of the body does not change, the gap is constant with time; that is, $\frac{d\Delta}{dt} = 0$. The term, $\frac{dm_y^*}{dh}$, can be expressed as given in Eq. (10). Then,
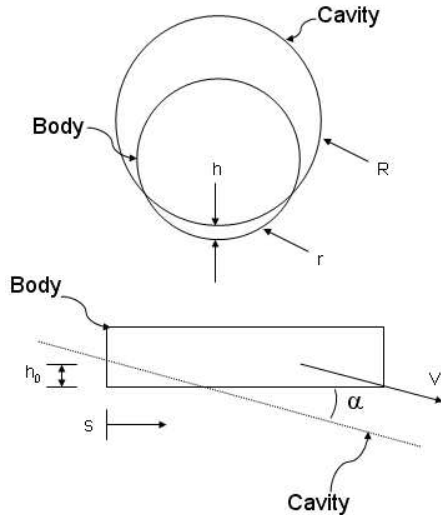
Fig. 5. Diagram of a cylinder planing on a cylindrical surface

the total planing force can be obtained by integrating over the entire wetted area as shown in Eq. (11), with $V_y = \dot{h}$.

For the supercavitating vehicle system, the planing force can be integrated using Eq. (11) for any cavity shape and any cavity to body orientation. For the case of a cylindrical body in steady planing along a cylindrical cavity, the cavity axis is parallel to the vehicle's velocity direction and the planing force can be represented as given by Eq. (12). For this case of steady planing, the immersion rate $\dot{h}$ along any section of the cavity is expressed as $V \sin(\alpha)$. The h_0 term is the immersion depth at the aft of the vehicle, as depicted in Fig. 5. The force centroid can also be calculated to be as given in Eq. (13), where X_P is the distance measured from the aft of the vehicle. The Paryshev planing force representation was chosen, as it has been shown to provide a good fit to experimental planing force data [17].

$$F_P = \pi \rho r^2 V^2 \sin(\alpha) \cos(\alpha) \left(1 - \frac{\Delta^2}{(h_0 + \Delta)^2} \right), \quad (12)$$

$$X_P = \left(\frac{h_0}{\text{tg}\,(\alpha)} \right) \left(\frac{h_0 + \Delta}{h_0 + 2\Delta} \right). \quad (13)$$

2. CONSIDERATION OF DELAY

The goal of this section is to explore the effects of the system delay along with the steady planing assumption. In much of the previous research, planing force modeling assumes steady planing in order to si-

mplify the planing force calculations. For calculations carried out with this assumption, any planing force contributions due to the vehicle motions into or out of the cavity are ignored. The planing force is then just a function of the wetted area, which is fully defined by the position of the body relative to the cavity. As the steady planing assumption leads to a purely positional dependent description of planing force, with this assumption damping relationships in terms of the vehicle's motion are not incoporated.

The steady planing assumption pertains to how the immersion rate term $\dot{h}$ is handled. With steady planing, along any wetted section, there is still an immersion rate that relates to the fact that the body is moving along the cavity axis at an angle. As discussed in Section 1.2, for steady planing, the immersion rate at any section of planing can be represented as $\dot{h} = V_t \cdot \sin(\alpha)$, where α is the angle between the body and the cavity, and V_t in this expression represents the total vehicle speed (Fig. 5). This immersion rate term does not include any radial motions of the body into the fluid.

Another important aspect with planing force modeling is the location and position of the cavity. Cavity shape and location predictions can have a significant effect on the resulting dynamics [8, 18, 19]. Two methods of modeling cavity position and orientation (with respect to the vehicle body) are shown in Fig. 6. At each instant in time as the cavitator moves through the fluid, the cavitator generates a vaporous cavity section that is centered about its current position. Each cavity section expands and contracts in a direction perpendicular to the cavitator velocity and each cavity section's growth can be assumed to occur independently, as proposed by Logvinovich [1]. With this, the cavity at the rear of the vehicle (where planning occurs) is actually generated by previous motions of the cavitator through the fluid. As such, the appropriate method of representing the cavity for planing is to model the cavity centerline and orientation based on previous cavitator position and velocity information. This is illustrated as the delayed approach in Fig. 6. In modeling in this manner, the planing force is dependent on the previous states and this complicates integration of the system dynamics. To avoid this, one common simplification is to use an instantaneous approach, where the cavity position and orientation is calculated based on the current cavitator position and velocity direction. In this approach, one approximates the cavity at the rear of the vehicle where planing occurs as a cavity that would have been generated if the cavitator had been steadily moving along its current velocity direction. This approximation works

V. Nguyen, B. Balachandran

well at capturing the dynamics of the system when the vehicle speeds are high or when the vehicle path is relatively straight. However this assumption may not properly account for the cavity-vehicle interactions when the vehicle speeds are low or when the vehicle is maneuvering.

In this work, the authors present a model in which they utilize both a delayed cavity approach to generate cavity location and orientation for planing, as well as a planing force formulation that includes vehicle motions into or out of the fluid. For simplification and computational purposes, the cavity is generated based on a single previous cavitator position and velocity direction. The time delay τ is chosen as L/V seconds, which represents approximately the time the vehicle takes to travel one body length. The section of the cavity generated by this previous cavitator orientation is used to define a cylindrical surface for the planing force calculation.
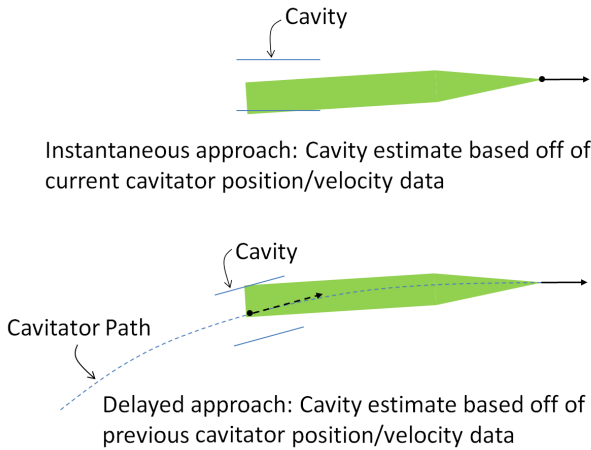

Fig. 6. Two methods of modeling cavity position and orientation

2.1. Description of immersion terms

A depiction of the cavity and vehicle centerlines in a general position is shown in Fig. 7. Since the cavity orientation is related to the previous position and velocity direction of the cavitator, there may be a positional offset between the cavity centerline and the nose of the vehicle, as well as a relative angle between the body centerline and the cavity centerline. In this figure, the cavity center is located at a previous nose position of (x_τ, z_τ). The cavity expands in a radial direction normal to the velocity direction at the previous time, making the cavity axis parallel to the delayed velocity direction. The cavity axis angle
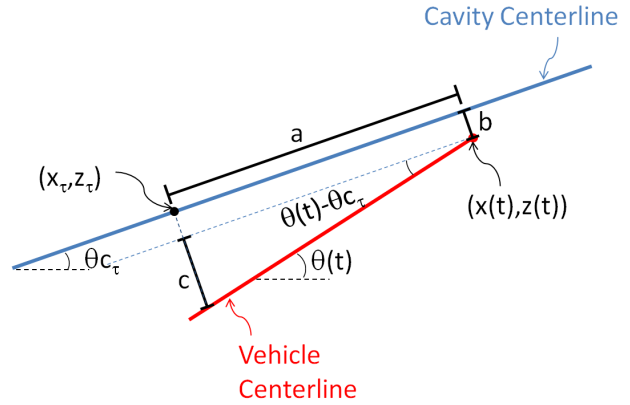

Fig. 7. Cavity and vehicle centerlines for the delayed case

with respect to horizontal is denoted as θc_τ and can be expressed as in Eq. (14). In this expression, the previous velocity direction can be defined by the sum of the delayed velocity angle with respect to the body (which can be calculated as $\mathrm{tg}^{-1}(w_\tau/V)$), and the delayed body orientation with respect to horizontal θ_τ.

$$\theta c_\tau = \theta_\tau - \mathrm{tg}^{-1}(w_\tau/V). \qquad (14)$$

The relative position of the aft of the vehicle with respect to the cavity centerline is a function of both a body translation and a body rotation. The radial translation of the current position of the nose with respect to the cavity centerline is expressed as b. The relative angle between the current body centerline and the cavity centerline can be expressed as $\theta(t) - \theta c_\tau$, where $\theta(t)$ is the current body orientation with respect to horizontal. The radial displacement due to body rotation, c, can be expressed as given in Eq. (15). The radial displacement of the body centerline at the rear with respect to the cavity at (x_τ, z_τ) is $b + c$.

$$c = a \cdot \mathrm{tg}\left(\theta(t) - \theta c_\tau\right). \qquad (15)$$

The immersion depth h can then be described as in Eq. (16), where $\Delta = Rc - R$. The immersion rate can then be generated by differentiating Eq. (16), which results in Eq. (17). The delay terms are treated as having no dependence on time, since they are only used to define an instantaneous stationary section of cavity on which the vehicle is planing. With the exception of expansion and contraction along the cavity radial direction, this instantaneous cavity does not move or change. This treatment corresponds to the physical phenomenon that the cavity is not moving in space once created; that is, it is simply expandi-
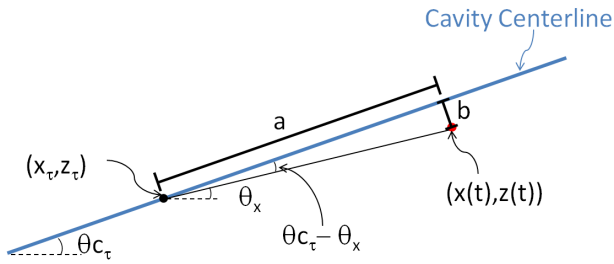
Fig. 8. Parameters a and b in relation to cavity centerline

ng or contracting.

$$h = a \cdot \text{tg}\,(\theta(t) - \theta c_\tau) + b - \Delta, \qquad (16)$$

$$\dot{h} = a \cdot \sec^2(\theta(t) - \theta c_\tau) \cdot q(t) + \dot{a} \cdot \text{tg}\,(\theta(t) - \theta c_\tau) + \dot{b} - \dot{R}c. \qquad (17)$$

The terms $\dot{a}$ and $\dot{b}$ represent the motion of the vehicle nose relative to the fixed cavity. These terms are the axial and radial components of the nose velocity with respect to the cavity axis. Returning to the immersion rate expression of Eq. (17), the first term relates to the rotation of the body into the cavity, the second term relates to the fact that the body is moving through the cavity with a relative angle, the third term relates to the rigid body motion of the vehicle into the fluid, and the last term relates to the cavity radial growth rate.

The parameters a and b can be solved by using geometry. In Fig. 8 the orientation of a and b, along with (x_τ, z_τ) and $(x(t), z(t))$, are shown. The line segment that joins (x_τ, z_τ), and $(x(t), z(t))$, creates an angle of $\theta_x = \text{tg}^{-1}\left(\dfrac{z_\tau - z(t)}{x(t) - x_\tau}\right)$ with the horizontal; it is noted that the numerator is $z_\tau - z(t)$ since z is positive in the downward direction. The relative angle that this segment creates with the cavity axis is $\theta c_\tau - \theta_x$. The parameters a and b can then be expressed as provided in Eqs. (18)–(19). By expanding the sin and cos terms, the expressions can be simplified to Eqs. (20)–(21). The rate of change can then be expressed as in Eqs. (22-23). As described earlier, these terms can similarly be considered as the axial and radial components of the vehicle velocity at the nose with respect to the cavity axis

$$\begin{aligned} a = & \sqrt{(z_\tau - z(t))^2 + (x(t) - x_\tau)^2} \times \\ & \times \cos\left(\theta c_\tau - \text{tg}^{-1}\left(\frac{z_\tau - z(t)}{x(t) - x_\tau}\right)\right), \quad (18) \end{aligned}$$

$$\begin{aligned} b = & \sqrt{(z_\tau - z(t))^2 + (x(t) - x_\tau)^2} \times \\ & \times \sin\left(\theta c_\tau - \text{tg}^{-1}\left(\frac{z_\tau - z(t)}{x(t) - x_\tau}\right)\right), \quad (19) \end{aligned}$$

$$a = \cos(\theta c_\tau)(x(t) - x_\tau) + \sin(\theta c_\tau)(z_\tau - z(t)), \quad (20)$$

$$b = \sin(\theta c_\tau)(x(t) - x_\tau) - \cos(\theta c_\tau)(z_\tau - z(t)), \quad (21)$$

$$\dot{a} = \dot{x} \cdot \cos(\theta c_\tau) - \dot{z} \cdot \sin(\theta c_\tau), \qquad (22)$$

$$\dot{b} = \dot{x} \cdot \sin(\theta c_\tau) + \dot{z} \cdot \cos(\theta c_\tau). \qquad (23)$$

As an aside, the impacting planing force expressions can be solved for the non-delayed or instantaneous case. In the case with no delay, the cavity is directly related to the current conditions at the nose, and the axis of the cavity is oriented along the current velocity direction. For no delay, $\theta_\tau = \theta(t)$, $w_\tau = w(t)$, $z_\tau = z(t)$, and $b = \dot{b} = 0$. The expression for the immersion depth becomes $h_{non\_delay} = a \cdot w/V - \Delta$ where V is the forward vehicle speed, as used in the vehicle dynamics modeling. The immersion rate simplifies to $\dot{h}_{non\_delay} = a \cdot \sec^2(\text{tg}^{-1}(w/V)) \cdot q + \dot{a} \cdot w/V - \dot{R}c$, where $\dot{a}$ is the total vehicle speed.

2.2. Integration into dynamics model

In order to incorporate the delay, the overall vehicle path needs to be accurately tracked in the inertial frame. The small angle assumptions can be removed from the propagation of the depth state, z, and an additional state for the x position can be added to the equations of motion represented by Eqs. (1) and (2). The expressions for $\dot{z}$ and $\dot{x}$ are given in Eqs. (24) and (25).

$$\dot{z} = w \cdot \cos(\theta) - V \cdot \sin(\theta), \qquad (24)$$

$$\dot{x} = V \cdot \cos(\theta) + w \cdot \sin(\theta). \qquad (25)$$

The planing force is calculated from the Paryshev representation [16]. The resulting planing force is represented as shown in Eq. (26), where $\Delta = R_c - r$, and h_0 is the immersion depth at the aft of the vehicle, as shown in Fig. 5.

$$F_P = \pi \rho r^2 \dot{h}^2 \frac{1}{\text{tg}\,(\alpha)} \left(1 - \frac{\Delta^2}{(h_0 + \Delta)^2}\right). \qquad (26)$$

2.3. Comparison with results from previous delay models

The vehicle parameters have been chosen to match those available in the literature with $m = 2$, $R_n = 0.0191$ m, $R = 0.0508$ m, $L = 1.8$ m, $n = 0.5$, and $C_{x0} = 0.82$. Simulation runs have been carried out by using a feedback control law that was also chosen to

V. Nguyen, B. Balachandran
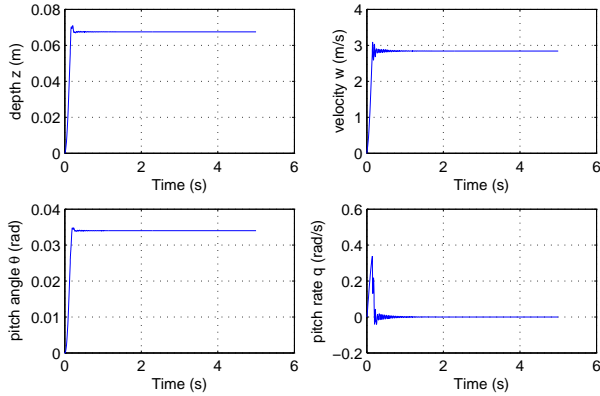
Fig. 9. Results for $\sigma = 0.0242$ and delayed system

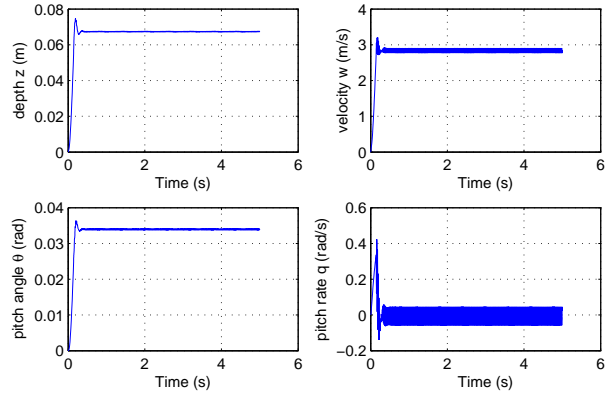Fig. 10. Results for $\sigma = 0.0242$ for non-delayed system, as $\tau \to 0$

match that from the literature and described by Eqs. (27).

$$
\begin{aligned}
\delta_e &= 0, \\
\delta_c &= 15z - 30\theta - 0.3q. \quad (27)
\end{aligned}
$$

The fins are assumed to be passive, while the cavitator input is utilized in a linear state feedback scheme. The feedback states are chosen such that they could be potentially measurable in practice. In the previous studies, this control law has been shown to exhibit both stable and limit-cycle planing motion depending on the vehicle speeds [3, 5, 6, 8, 18, 19].

Results obatined from a simulation conducted for the delayed system at $\sigma = 0.0242$ ($V = 83.51$ m/s) are shown in Fig. 9. The delay formulation requires information about previous positions, so the simulation is seeded with initial condition assuming the vehicle has been traveling along a straight and level trajectory. Due to gravity, the aft end of the vehicle dips into the cavity, and eventually, the system displays stable planing behavior at this speed. However, similar to what has been observed in previous supercavitating vehicle dynamics simulations, when the authors utilize the same feedback formulation [3, 6, 7], the vehicle response exhibits oscillations as the speed is decreased (i.e., an increase in cavitation number σ) and the cavity becomes tighter around the vehicle.

The instantaneous cavity approach, which is illustrated in Fig. 6), can also be modeled by allowing the delay value to approach 0. Results for the delay-free case in the presence of non-steady planing are shown in Fig. 10. This simulation has been conducted for a cavitation number of $\sigma = 0.0242$ ($V = 83.51$ m/s), and the system response is oscillatory. The results for this particular speed are

presented, since this is the opposite of what has been observed in previous delay studies with steady planing assumptions [12]. In the earlier studies, the introduction of the delay was found to be destabilizing.

It should be noted that for sufficiently high speeds (or equivalently, low cavitation numbers), the systems with and without delay exhibits stable behavior. As the cavitation number is increased (i. e., speed is decreased), both the delayed and non-delayed systems transition from stable fixed-point motions to limit-cycle motions. However, the transition for the non-delayed system occurs at a slightly higher speed. It is within this window that the delayed system and the non-delayed system demonstrate differing behavior.

If the delay is taken as a parameter, and the forward velocity is held constant at $V = 83.51$ m/s, a projection of resulting steady-state behavior on the $w - q$ plane is as illustrated in Fig. 11. Here, the delay is varied from close to 0 s (no delay), to 0.02156 s (the nominal delay value of L/V). The system can be seen to transition from a limit-cycle motion to an asymptotically stable equilibrium position, as the delay is increased. By varying the delay with a fine timestep of less then 0.00001 s, the critical value of $\tau = 0.01750$ s is found; for the chosen vehicle speed, limit cycles exist for $\tau < 0.01750$ s.

3. MANEUVERING STUDIES

Appropriate tracking of the vehicle's inertial orientation is required in order to incorporate the delay and non-steady planing effects. The modifications made to the vehicle dynamics model inherently
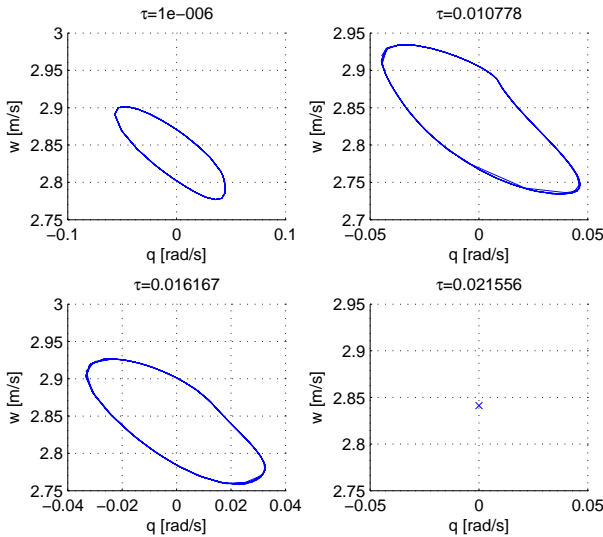
Fig. 11. Effect of delay on long-time system response

Fig. 12. Depiction of inner and outer loop controllers

are not straight and level

$$\delta_{c\_inner} = k_{inner}q. \qquad (28)$$

The feedback controller has the purpose of mitigating fast time-scale disturbances, while an outer-loop controller is used to help guide the vehicle along the desired maneuver. A diagram of how the two controllers are integrated is illustrated in Fig. 12.

The outer-loop control is determined by an optimization, which takes into account the desired maneuver and the vehicle dynamics. Control parameters that are used to define a control input function are treated as variables in an optimization scheme. The system dynamics are directly integrated and the maneuver itself is treated as a constraint on the optimization, thus, constraining the dynamics to conform to the desired maneuver. The control inputs can than be optimized for total time (which can also be treated as a variable) or ending state, depending on the type of maneuver considered.

In this work, the type of motion considered is a move-to-point or homing maneuver. The goal of the maneuver is to move to some desired end position given some initial position and states. The authors used the optimization scheme to search for the outer-loop control inputs that helps accomplish this motion in the shortest possible time. The basic optimization formulation can be described as follows. The maneuver is divided into s time intervals, and the control inputs are defined over each discrete interval as shown in Fig. 13. The objective function can be expressed as in Eq. (29). The optimization variables are the final time T, and the u_is, which are the parameters used to define the control input over each discrete interval. In the simplest case, the control can be assumed as constant over each interval, and in this situation, u_i would represent the constant control value (the cavitator actuation angle and the fin actuation angle) over interval i. This function is subject to the constraint shown in Eq. (30), where x_f is the desired final state that is defined by the maneuver. The state values at end of each of the time interval, can be calculated as shown in Eq. (31), for $i = 1...s$ and given x_0. The integration of $F(t, x, u_i)$ is determined by integrating the equations of motion.

removed the inertial small angle assumptions in the equations of motion. These assumptions were appropriate in previous studies since only fixed points were generally considered. However, inertial tracking opens the door for steady motions such as those that occur during maneuvering. This may be important for characterizing vehicle capabilities.

Maneuverability for non-linear systems, and particularly for non-smooth systems, can be difficult to characterize since an "all out", fully saturated control inputs do not necessarily define the envelope of vehicle motion capabilities. Supercavitating vehicles are a good representative example, since fully saturated control inputs can push the system into tailslap behavior, which negatively affects the position control of the vehicle. In this study, a numeric direct optimal control approach is used, and in this approach, the authors search for optimal controller inputs for defined vehicle maneuvers. Due to the complexity of the supercavitating vehicle system, a numerical approach is needed.

A feedback controller is utilized in order to reject fast time-scale instabilities, such as due to the planing force. State feedback control as shown in Eqs. (27) has been shown to stabilize the vehicle for straight and level travel. However, an utilization of feedback about the inertial positions z and θ can be detrimental to maneuvering along complex paths. Instead, the inertial terms can be dropped and an inner-loop control of the form as shown in Eq. (28) can be utilized. This type of controller still aids in stabilizing the system while allowing for travel along paths that
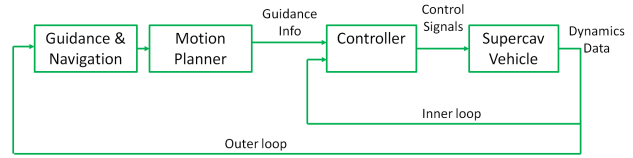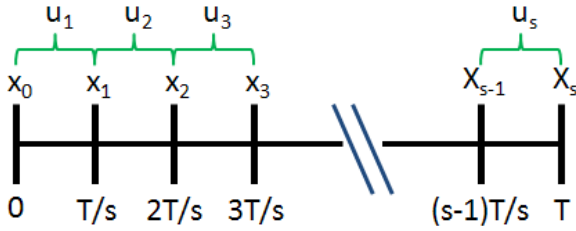
V. Nguyen, B. Balachandran

Fig. 13. Discretization method for the optimization strategy used to generate controller input

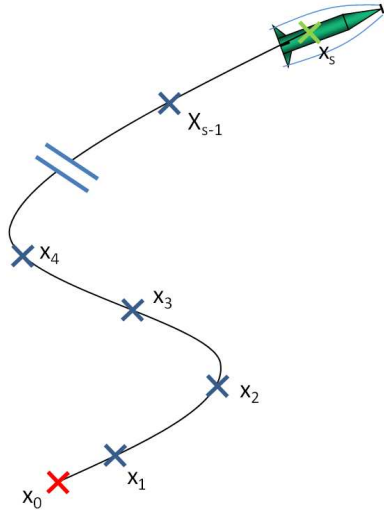Fig. 15. Vehicle path with delayed, non-steady planing force model, for run to $(z_f, x_f) = (-20, 80)$

Fig. 14. Diagram of trajectory generated using the constant control inputs over discretized time segments

A depiction of the resulting maneuver is illustrated in Fig. 14

$$min_{u_1, u_2, \ldots, u_s, T}(T), \qquad (29)$$

$$x_s = x_f, \qquad (30)$$

$$x_i = \int_{t=(i-1)T/s, x_{i-1}}^{t=iT/s} F(t, x, u_i)dt. \qquad (31)$$

The bounds on the control are easily applied as bounds on the optimization variables, and additional constraints can be added to bound the states or refine the maneuver. With the dynamics and the constraints, the optimization can become quite complex. Simple search algorithms based on penalty methods to enforce the constraints were found to be the most effective at finding good solutions. A more detailed discussion of the optimization formulation is presented in the first author's dissertation [19].

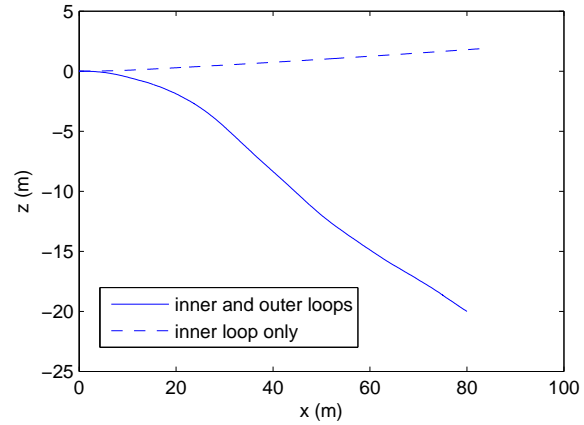For the following maneuvers, the inner-loop gain is set at $k_{inner} = -0.9$, and the cavitation number

is chosen as $\sigma = 0.03$ which equates to a forward speed of $V = 75$ m/s. The control function is defined as a spline interpolation of control values at s equally spaced discrete points throughout the maneuver. The control values at these discrete points are the parameters u_i, which are solved for through the optimization scheme. This formulation generates a smooth outer-loop control input. The discrete control actuation angles are limited to $\delta_{c/e} \leq \pi/2.5$, and in order to maintain small vehicle slip angles, the maximum allowable transverse speeds during the maneuver is constrained to $|w| \leq 6$ m/s. The maneuver is discretized into $s = 14$ segments. A move-to-point maneuver is shown in Fig. 15. The vehicle begins with straight and level flight at point $(x, z) = (0, 0)$ m at time $t = 0$ s. The desired end point is at $(x_f, z_f) = (80, -20)$ m. The resulting outer-loop control inputs are shown in Fig. 16. The optimization is seeded with an initial guess of 0 control input with an arbitrary end time of 0.8 s. The maneuver takes 1.1047 s. The resulting state time histories are shown in Fig. 17. The vehicle can be seen to change angle of attack throughout the maneuver as the transverse velocity and pitch rate change signs.

The move-to-point maneuver can also be considered with an obstacle or no-fly zone. Such a maneuver is shown in Fig. 18. The vehicle again is assumed to begin with straight and level travel at point $(x, z) = (0, 0)$ m at time $t = 0$ s with a desired endpoint of $(x_f, z_f) = (80, -20)$ m. A circular no-fly zone is added and is centered at $(x_{obst}, z_{obst}) = (40, -5)$ m with a radius of $r_{obst} = 5$ m. The obstacle is placed so that it interferes with the optimal trajectory found for the obstacle free case. The circular no-fly zone can be integrated as a
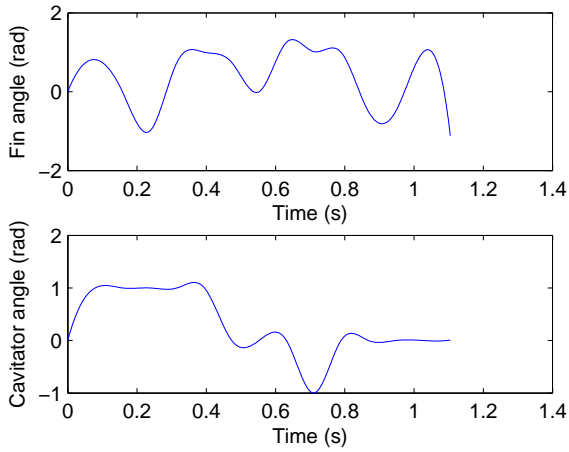
Fig. 16. Outer-loop Control inputs for delayed, non-steady planing force model and run to $(z_f, x_f) = (-20, 80)$ m
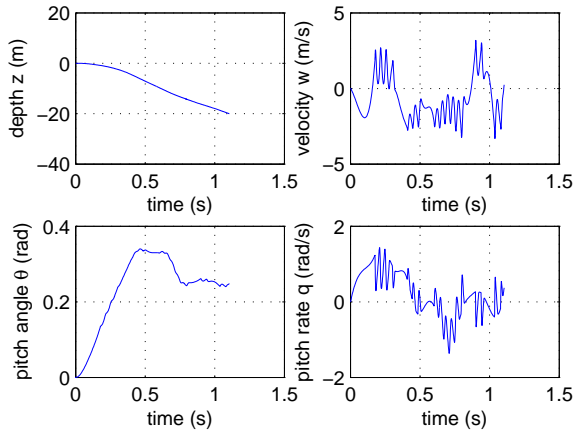

Fig. 17. State time histories with delayed, non-steady planing force model, for run to $(z_f, x_f) = (-20, 80)$ m
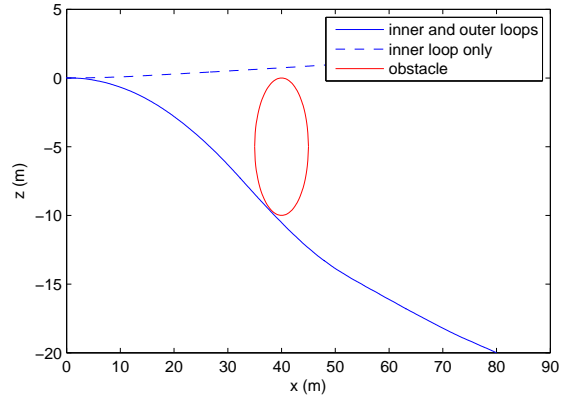

Fig. 18. Vehicle trajectory with delayed, non-steady planing force model, for run to $(z_f, x_f) = (-20, 80)$ m with obstacle at $(z_{obst}, x_{obst}) = (-5, 40)$, $r_{obst} = 5$ m
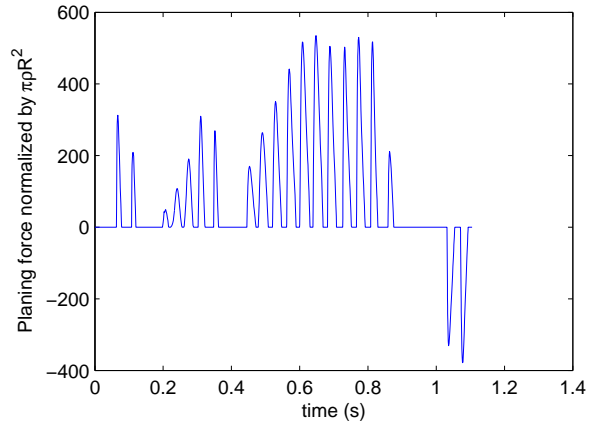

Fig. 19. Planing run for delayed, non-steady planing force model, for run to $(z_f, x_f) = (-20, 80)$ m with obstacle at $(z_{obst}, x_{obst}) = (-5, 40)$, $r_{obst} = 5$ m

single constraint on the minimum distance between vehicle trajectory and obstacle center as shown in Eq. (32). Solutions were also found for smaller obstacle radii and the 5 m obstacle approaches the largest obstacle in which the search algorithm could find an adequately feasible solution. The optimization scheme can be sensitive to the initial guesses, and both 0 seeds and previous solution seeds (using a known feasible solution for a similar maneuver) were attempted. This allowed for trajectories both above and below the obstacle to be considered. The resulting trajectory was a slight modification from the obstacle free case but the total maneuver time is not heavily affected with the resulting maneuver taking

1.1050 s

$$r_{obst} \leq \min_t \sqrt{(x(t) - x_{obst})^2 + (z(t) - z_{obst})^2}. \quad (32)$$

A plot of the planing force throughout the maneuver is shown in Fig. 19. The body is clearly seen to be making intermittent contact with the cavity surface. The change in direction of the planing force shows a switch of planing surfaces as the trajectory curvature changes throughout the maneuver. The contact arises from the aggressive maneuvering dictated by the obstacle size, endpoint location, and time optimization.

For comparative purposes, results obtained for a steady planing, instantaneous cavity simulation is shown in Fig. 20. This simulation was run by using the same conditions with $\sigma = 0.03$, $k_{inner} =$
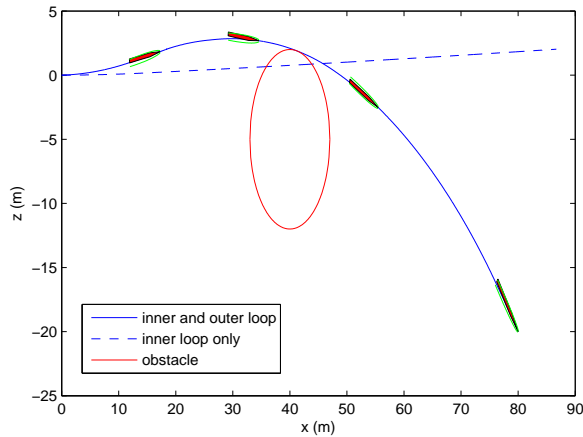
V. Nguyen, B. Balachandran

Fig. 20. Vehicle trajectory with non-cylindrical steady planing model without delay, for run to $(z_f, x_f) = (-20, 80)$ m with obstacle at $(z_{obst}, x_{obst}) = (-5, 40)$, $r_{obst} = 7$ m

-0.9, $(x_f, z_f) = (80, -20)$ m, and $(x_{obst}, z_{obst}) = (40, -5)$ m. To conduct this simulation, the authors utilized the same cavity model, and a non-cylindrical planing force model as described in the authors' previous work [8]. With the instantaneous assumption, the cavity orientation is directly related to the current body orientation, and as such real-time cavity orientations can be easily produced. Plots of the vehicle and cavity orientations at points along the trajectory are included here for better visualization; the size has been exaggerated for illustrative purposes. Here feasible solutions are found for a much larger obstacle of $r_{obst} = 7$ m. This difference hints at the limiting nature of properly incorporating the delay and non-steady planing effects.

CONCLUDING REMARKS

The authors have presented a method to appropriately account for vehicle body motion into the cavity during planing in the presence of time-delay effects. In previous studies, cavity interaction forces have been estimated on the basis of the planing force present during steady planing. Simulations are carried out by utilizing a cavitator feedback law used in prior efforts [3, 5, 6, 8, 12]. A transition from steady planing to oscillatory motion is observed as cavitation number is increased (i.e., speed and cavity size is decreased). This transition can be similarly observed in other vehicle dynamics simulations with various assumptions. However, the dynamic behavior for these systems can vary greatly when transitioning between different regions of operati-

on. As such, high-fidelity models are desired when attempting to accurately predict vehicle motions. The current interaction model is also compared to a previous time-delay model in which the steady planing assumption has been utilized. Contrary to the previous study, the simulation results presented here show that for a particular window of cavitation numbers, incorporating the delay has a stabilizing effect on the system dynamics.

The new interaction modeling requires accurate inertial tracking of the cavity and body. A detailed methodology is presented to properly account for the cavity time-delay effects. These effects are caused by the physical delay due to the fact that the cavity at the aft end of the vehicle where planing occurs relates to previous locations and orientations of the cavitator. Also, removed are small angle assumptions that were valid in previous studies of near fixed-point operation (straight and level flight). The resulting vehicle dynamics model is more general than previous formulations and this generality allows for studies of dynamic maneuvering which include motions and angles that deviate greatly from steady-state operations. Maneuvers were considered by using a numeric optimizer to generate outer-loop control inputs while a simple feedback controller was used to mitigate fast disturbances. Advantageous use of planing is made in the resulting optimized trajectories, and this idea of using planing for vehicle operations can be traced back to the studies of Logvinovich. The current work can be used as a basis for studying the maneuverability of different supercavitating vehicles.

1. *Logvinovich G.V.* Hydrodynamics of Free-Boundary Flows.– Translated from Russian: Kiev, 1969.– 208 p.

2. *Logvinovich G.V.* Some problems in planing surfaces // Trudy TsAGI, Translated from Russian.– 1980.– Vol. 2052.– P. 3–12.

3. *Dzielski J., and Kurdila A.* A benchmark control problem for supercavitating vehicles and an initial investigation of solutions // Journal of Vibration and Control.– 2003.– Vol. 9.– P. 791–804.

4. *Kulkarni S.S., and Pratap R.* Studies on the dynamics of a supercavitating projectile // Applied Mathematical Modelling.– 2000.– Vol. 24, N2.– P. 113–129.

5. *Lin G., Balachandran B., and Abed E.* Dynamics and control of supercavitating vehicles // ASME Journal of Dynamic Systems, Measurements, and Control.– 2008.– Vol. 130.– P. 021003-1–021003-11.

6. *Lin G., Balachandran B., and Abed E.* Nonlinear dynamics and bifurcations of a supercavitating vehicle // IEEE Journal of Oceanic Engineering.– 2007.– Vol. 32.– P. 753–761.

7. *Lin G., Balachandran B., and Abed E.* Absolute stability of second-order systems with asymmetric sector boundaries // IEEE Transactions on Automatic Control.– 2010.– Vol. 55, N 2.– P. 458–463.

V. Nguyen, B. Balachandran

8. *Nguen V., and Balachandran B.* Supercavitating vehicles with noncylindrical, nonsymmetric cavities: Dynamics and instabilities // ASME Journal of Computational and Nonlinear Dynamics.– Vol. 6, N 4.– 2011.– P. 041001-1–041001-11.

9. *Kirschner I., Kring D.C., Stokes A.W., Fine N.E., and Uhlman J.S.* Control strategies for supercavitating vehicles // Journal of Vibration and Control.– 2002.– Vol.8, N 2.– P. 219–242.

10. *Kirschner I., Uhlman J.S., and Perkins J. B.* Overview of High-Speed Supercavitating Vehicle Control // AIAA Guidance, Navigation, and Control Conference and Exhibit.– 2006.– Keystone.– P. Colorado USA.

11. *Vanek B., Bokor J., Balas G. J., and Arndt R. E.* Longitudinal motion control of a high-speed supercavitation vehicle // Journal of Vibration and Control.– 2007.– Vol.13, N 2.– P. 159–184.

12. *Hassouneh M. A., Nguyen V., Balachandran B., and Abed E. H.* Stability analysis and control of supercavitating vehicles with advection delay // ASME Journal of Computational and Nonlinear Dynamics.– 2013.– Vol.8, N 2.– P. 021003–021013.

13. *Choi J.-Y., Ruzzene M., and Bauchau O.A.* Dynamic analysis of flexible supercavitating vehicles using modal-based elements// SIMULATION.–2004.–

Vol.80, N 11.– P. 619–633.

14. *Ruzzene M., Kamada R., Bottasso C.L., and Scorcelletti F.* Trajectory optimization strategies for supercavitating underwater vehicles // Journal of Vibration and Control.– 2008.– Vol.14, N 5.– P. 611–644.

15. Ahn S.S. An integrated approach to the design of supercavitating underwater vehicles // PhD Dissertation, Georgia Institute of Technology, August 2007.

16. Paryshev E.V. Mathematical modeling of unsteady cavity flows // Proc. Fifth International Symposium on Cavitation (CAV2003), 2003, Osaka, Japan.

17. Dzielski J. Planing model discrepancies. Private communication, 2004.

18. *Nguyen V., Balachandran B., and Varghese A. N.* Supercavitating vehicle dynamics with non-cylindrical, non-symmetric cavities // Proc. ASME International Mechanical Engineering Congress and Exposition.– 2007.– Seattle, WA, USA.– P. 265-272.

19. Nguyen V. Dynamics and control of non-smooth systems with applications to supercavitating vehicles // PhD Dissertation, University of Maryland, August 2011.

V. Nguyen, B. Balachandran